Ion–Molecule Association Reactions: Reaction Sequences Initiated by $CH_3OH_2^+$ in CH_3OH; Experiment and Theory

Lewis M. Bass, R. Dwight Cates, Martin F. Jarrold, Nicholas J. Kirchner, and Michael T. Bowers*

Contribution from the Department of Chemistry, University of California, Santa Barbara, California 93106. *Received December 27, 1982*

Abstract: Protonated methanol reacts with CH_3OH at low pressures to form primarily protonated dimethyl ether and water at about 5% of the collision rate. As the pressure increases, clustering of $CH_3OH_2^+$ with CH_3OH competes with H_2O elimination, and at higher pressures still further clustering of the protonated methanol dimer and of protonated dimethyl ether occurs. The rate constants for these processes have been measured as a function of temperature and pressure with the use of ion cyclotron resonance spectroscopy. A metastable reaction is observed in the second field free region of a reverse geometry mass spectrometer for loss of H_2O from nascent $(CH_3OH)_2H^+$ collision complexes. The kinetic energy release distribution was measured for the metastable yielding an average release of 75 meV. The system was modeled by using statistical phase space theory with generally good agreement found between theory and experiment.

I. Introduction

Ion–molecule association reactions have received an increasing amount of attention in recent years. The largest part of this attention has been focused on determining equilibrium thermodynamic properties of various clusters,[1,2] with much less known about the kinetic mechanisms of cluster formation itself.[3] We have chosen to focus on this latter aspect of the problem, in particular on the first step in the clustering phenomena. Our initial work[4,5] dealt with the formation of proton bound dimers in simple amines

$$RH^+ + R \rightarrow R_2H^+ \qquad (1)$$

for R = NH_3, CH_3NH_3, $(CH_3)_2NH$, and $(CH_3)_3N$. These systems were chosen because the only reaction that occurs is simple clustering, and we felt it would be possible to develop accurate theoretical models to test against experiment. A simple energy-transfer mechanism had been proposed by Moet-Ner and Field[6] for reaction 1, and RRKM calculations performed by Olmstead et al.[7] seemed to fit the data well. Our contribution was to measure[4] the association rate constants and their temperature dependence at much lower pressures than Moet-Ner and Field and to develop a phase space theory model for clustering that rigorously conserved energy and angular momentum.[5]

It is of interest to extend the simple clustering model in two ways. First, it is necessary to determine the effect of competing reaction channels on clustering. There are two general types to be considered: radiative stabilization processes and molecular/atomic elimination processes. We have recently published both experimental[8,9] and phase space theoretical modeling[9] on the reaction

$$CH_3^+ + HCN \rightarrow (CH_3{\cdot}HCN)^+ + h\nu \qquad (2)$$

Important theoretical work on radiative stabilization has also been published by Dunbar,[10] Woodin and Beauchamp,[11] and Herbst.[12] Molecular elimination competing with back dissociation or collisional stabilization will be one of the main points of this paper.

The second extension necessary in understanding clustering is to begin to model sequential clustering. In general this will require incorporating a detailed energy-transfer model into the existing association theory formalism. Such a model is required but awaits future development. In this paper we will report experimental data on higher order clustering and present a simplified model for dealing with it.

The system we have chosen to investigate is the ionic clustering in methanol. The clustering is initiated by protonated methanol, an ion that is rapidly formed from methanol parent ions by proton transfer.[13]

$$CH_3OH^+ + CH_3OH \xrightarrow{2 \times 10^{-9}\ cm^3/s} CH_3OH_2^+ + CH_3O \qquad (3)$$

The protonated methanol ion then reacts much more slowly with CH_3OH to form either the proton bound dimer or the protonated dimethyl ether[14] by H_2O elimination from the collision complex. These two processes compete on the time, pressure, and temperature scales experimentally available to us. The methanol dimer undergoes further clustering to form trimer, tetramer, etc., and the protonated ether forms a mixed ether–methanol proton bound dimer. The qualitative features of the reactions in methanol have been reported in some very nice early work of Henis.[15]

The phenomenological rate constants that are of interest to us here are summarized in the following reactions:

$$CH_3OH_2^+ + CH_3OH \xrightarrow{k_{DIM}} (CH_3OH)_2H^+ \qquad (4)$$

$$CH_3OH_2^+\ CH_3OH \xrightarrow{k_{H_2O}} (CH_3)_2OH^+ + H_2O \qquad (5)$$

$$(CH_3OH)_2H^+ + CH_3OH \xrightarrow{k_{TRI}} (CH_3OH)_3H^+ \qquad (6)$$

$$(CH_3)_2OH^+ + CH_3OH \xrightarrow{k_{AHB}} [(CH_3)_2O]H^+[CH_3OH] \qquad (7)$$

These reactions and the associated rate constants are the exper-

(1) P. Kebarle, "Modern Aspects of Electrochemistry", Vol. 9, E. Conway and J. O. M. Bockris, Eds., Plenum Press, New York, 1973, pp 1–46.
(2) P. Kebarle, *Annu. Rev. Phys. Chem.*, **28**, 445 (1977).
(3) A. W. Castleman, *Adv. Colloid Interface Sci.*, **7** (1977); P. Ausloos, Ed., "Kinetics of Ion–Molecule Reactions", Plenum Press, New York, 1979, pp 295–321.
(4) P. V. Neilson, M. T. Bowers, M. Chau, W. R. Davidson, and D. H. Aue, *J. Am. Chem. Soc.*, **100**, 3649 (1978).
(5) L. Bass, W. J. Chesnavich, and M. T. Bowers, *J. Am. Chem Soc.*, **101**, 5493 (1979).
(6) M. Moet-Ner and F. H. Field, *J. Am. Chem. Soc.*, **97**, 5339 (1975).
(7) W. N. Olmstead, M. Lev-On, D. M. Golden, and J. I. Brauman, *J. Am. Chem. Soc.*, **99**, 992 (1977).
(8) M. J. McEwan, V. G. Anicich, W. T. Huntress, P. R. Kemper, and M. T. Bowers, *Chem. Phys. Lett.*, **75**, 278 (1980).
(9) L. M. Bass, P. R. Kemper, V. G. Anicich, and M. T. Bowers, *J. Am. Chem. Soc.*, **103**, 5283 (1981).
(10) R. Dunbar, *Spectrachim. Acta., Part A*, **31A**, 797 (1975).
(11) R. L. Woodin and J. L. Beauchamp, *Chem. Phys.*, **41**, 1 (1979).
(12) E. Herbst, *Ap. J.*, **205**, 94 (1976).
(13) M. T. Bowers, T. Su, and V. G. Anicich, *J. Chem. Phys.*, **58**, 5175 (1973).
(14) That protonated dimethyl ether is formed has been confirmed by collision-induced decomposition studies: M. F. Jarrold and M. T. Bowers, to be published.
(15) J. M. S. Henis, *J. Am. Chem. soc.*, **90**, 844 (1968).

0002-7863/83/1505-7024$01.50/0

imentally observed quantities. In order to be able to theoretically model them a microscopic mechanism must be proposed. We propose a mechanism that is a simple extension of that successfully applied to the amine system:[4-7]

$$AH^+ + A \underset{k_{b1}}{\overset{k_{f1}}{\rightleftharpoons}} (A_2H^+)^* \begin{cases} \xrightarrow{k_{s1}[A]} A_2H^+ & (8a) \\ \xrightarrow{k_{d1}} BH^+ + H_2O & (8b) \end{cases}$$

$$A_2H^+ + A \underset{k_{b2}}{\overset{k_{f2}}{\rightleftharpoons}} (A_3H^+)^* \xrightarrow{k_{s2}[A]} A_3H^+ \quad (9)$$

$$BH^+ + A \underset{k_{b3}}{\overset{k_{f3}}{\rightleftharpoons}} (AH^+B)^* \begin{cases} \xrightarrow{k_{s3}[A]} AH^+B & (10a) \\ \xrightarrow{k_{d3}} AH^+ + B & (10b) \end{cases}$$

where the notation A = CH_3OH and B = $(CH_3)_2O$ has been introduced for the sake of clarity. Each of the species denoted by an asterisk is assumed to be a short-lived intermediate complex. If this is the case, then a steady-state analysis can be used to related the phenominological rate constants to the microscopic rate constants:

$$k_{DIM} = \frac{k_{f1}k_{s1}[A]}{k_{b1} + k_{d1} + k_{s1}} \quad (11)$$

$$k_{H_2O} = \frac{k_{f1}k_{d1}}{k_{b1} + k_{d1} + k_{s1}[A]} \quad (12)$$

$$k_{TR1} = \frac{k_{f2}k_{s2}[A]}{k_{b2} + k_{s2}[A]} \quad (13)$$

$$k_{AHB} = \frac{k_{f3}k_{s3}[A]}{k_{b3} + k_{d3} + k_{s3}[A]} \quad (14)$$

The paper is organized as follows. Section II is the Experimental Section where details are given on how the phenomenological rate constants are measured. Section III contains the theoretical model that will be used to calculate the microscopic rate constants. This section will be followed by a brief Results section (IV) and then a Discussion section (V). The paper will conclude with a Summary section and a brief Appendix containing some technical information used in the calculations.

II. Experimental Section

All of the kinetic measurements were made on the UCSB drift cell ion cyclotron resonance (ICR) spectrometer. This spectrometer is equipped with a Baratron capacitance manometer for pressure measurement, and the cell is temperature variable over the range 100–450 K. The $CH_3OH^+\cdot$ ions are formed by electron impact at energies near threshold. No fragment ions are formed. At the temperatures and pressures of our experiment the $CH_3OH^+\cdot$ ions rapidly react with CH_3OH to form $CH_3OH_2^+\cdot$. These $CH_3OH_2^+\cdot$ ions then drift through the ICR cell and slowly react to form either $(CH_3)_2OH^+/H_2O$ or $(CH_3OH)_2H^+$ products. Typical reaction times are of the order of 1×10^{-3} s. The details of the spectrometer have been previously described in the literature,[16] and a further description will not be given here.

The UCSB ICR is equipped with marginal oscillator detection. As a consequence the ions are detected as a power absorption signal. Since ICR power absorption is a resonance phenomenon, it is interrupted when the ion undergoing observation suffers a collision, leading to line broadening. Because the experiments reported here spanned a wide pressure range, the general form of the power absorption equations must be used. In addition, the entire kinetic scheme must be incorporated into the power absorption scheme so that primary, secondary, and tertiary ions can be accounted for. The necessary equations have been developed by Kemper[17] and applied to the methanol system by Cates.[18] A discussion for the kinetically simpler amine association reactions has been given by Nielson et al.,[4] which exemplifies the general method used. No details will be given here.

The kinetic energy distribution in the water loss channel was obtained on a high-resolution, reverse-geometry mass spectrometer (V. G. Analytical ZAB-2F). This spectrometer is fitted when a home-built high-pressure temperature-variable ion source.[19] The proton-bound dimer of methanol was formed in the ion source, extracted, mass selected, and allowed to undergo metastable decomposition in the second field free region of the mass spectrometer. The kinetic energy distribution was obtained from the metastable peak shape, using techniques previously described.[19]

The methanol used was Aldrich AR grade and it was checked for impurities by using mass spectrometry. No impurities were detected.

III. Theory

A. Overall Perspective. The reaction scheme shown in eq 8–10 is comprised of three types of steps: collision of an ion with a molecule to form an excited complex; unimolecular dissociation of the complex, either back to reactants or forward to some product channel; and stabilization of the complex via nonreactive collisions with the neutral parent gas. These three steps will be discussed in general terms in this section. The incorporation of these steps into reactions 8, 9, and 10 will be discussed in sections IIIB, IIIC, and IIID, respectively.

The assumptions that provide the framework for modeling the three steps just listed can be summarized as follows:

(1) Ion–neutral collision rates are determined by passage across the centrifugal barrier in the long-range part of the effective potential. Thus, thermal ion–molecule collision rate constants can be calculated from classical Langevin theory[20a] for nonpolar neutrals or from ADO theory for polar molecules.[20b]

(2) All thermal energy ion–molecule collisions result in the formation of a collision complex. Thus, the rate constant for complex formation can be calculated according to assumption 1.

(3) All collisions of an excited complex with the neutral parent gas result in stabilization of the complex with regard to back-dissociation.

(4) The excited complex reaches a state of quasiequilibrium (energy randomization) before dissociating. Hence, subject only to restrictions imposed by conservation of energy and angular momentum, all states of the complex are populated uniformly.

(5) The rate of dissociation of the complex into any available fragment channel is determined by the corresponding rate of passage across the appropriate transition state in that channel. In terms of the system dynamics the transition state is defined as a dividing surface in the system phase space such that all reactive trajectories cross this surface once and only once and all nonreactive trajectories do not cross the surface at all.[21]

In order to satisfy the principle of microscopic reversibility the back-dissociation of the complex into the reactant channel must be described by the orbiting transition state located at the centrifugal barrier. Hence, both the formation of the complex and its back-dissociation are governed by the same transition state. Dissociation into other fragment channels may be described by orbiting or tight transition states, depending upon the nature of the process.

Assumption 3 is reasonable because the stabilizing bath gas is the neutral CH_3OH molecule. Hence, stabilization can efficiently take place via ligand switching or more usual forms of rotational/vibrational energy transfer. In the past very efficient energy transfer has been observed when ligand switching was a possible mechanism.[22] It should also be noted that only a very small amount of energy needs to be removed from the collision complex to keep it from back-dissociating to reactants.

(16) A. G. Wren, P. Gilbert, and M. T. Bowers, *Rev. Sci. Instrum.*, **498** 531 (1978); M. T. Bowers, P. V. Neilson, P. R. Kemper, and A. G. Wren, *Int. J. Mass Spectrom Ion Phys.*, **258** 103 (1978).

(17) P. R. Kemper, Ph.D. Thesis, University of California, Santa Barbara, CA, 1977.

(18) R. D. Cates, Ph.D. Thesis, University of California, Santa Barbara, CA, 1981.

(19) M. F. Jarrold, A. J. Illies, and M. T. Bowers, *Chem. Phys.*, **65**, 19 (1982).

(20) (a) P. Langevin, *J. Chim. Phys.*, **5**, 245 (1905); G. Gioumousis and D. P. Stevenson, *J. Chem. Phys.*, **29**, 294 (1958). (b) T. Su and M. T. Bowers, *J. Chem. Phys.*, **58**, 3027 (1973); *Int. J. Mass Spectrom Ion Phys.*, **17**, 309 (1975); L. Bass, T. Su, W. J. Chesnavich, and M. T. Bowers, *Chem. Phys. Lett.*, **34** 119 (1975).

(21) W. J. Chesnavich and M. T. Bowers in "Gas Phase Ion Chemistry", Vol. 1, M. T. Bowers, Ed., Academic Press, New York, 1979, pp 119–153; P. Pechukas in "Dynamics of Molecular Collisions", Part B, W. H. Miller, Ed., Plenum Press, New York, 1976.

(22) R. D. Cates and M. T. Bowers, *J. Am. Chem. Soc.*, **102**, 3994 (1980). A. J. Illies, M. F. Jarrold, and M. T. Bowers, *ibid.*, **105**, 2562 (1983).

Assumptions 4 and 5 provide the basis for statistical reaction rate theory, most commonly applied in the form of RRKM theory[23] or QET.[24] When the orbiting transition state is utilized and angular momentum conservation rigorously adhered to (in the classical limit), the formalism is usually referred to as "phase space" theory.[25] Several reviews of statistical theory have recently been presented.[21] The application of the phase space model to ion–molecule association reactions has been discussed previously.[5,9] Only the results that are of immediate interest in this work will be discussed here.

According to statistical theory as outlined in assumptions 4 and 5 the rate constant for unimolecular dissociation into a particular fragment channel is written as

$$k(E,J) = \frac{\Phi(E,J)}{\rho(E,J)} \tag{15}$$

where $\Phi(E,J)$ is the flux at the transition state and $\rho(E,J)$ is the density of states of the unimolecular reactant (in this case the excited complex). For the orbiting transition state this expression becomes

$$k(E,J) = \frac{S\int_{E_{tr}^*}^{E}[dE_{tr}\Gamma(E_{tr},J)\rho_v(E - E_0 - E_{tr})]}{2Jh\rho_v'(E - BJ^2)} \tag{16}$$

where S is the reaction path degeneracy factor, $\Gamma(E_{tr},J)$ is the rotational–orbital sum of states at translational–rotational energy E_{tr} and angular momentum J, $\rho_v(E - E_0 - E_{tr})$ is the vibrational density of states of the fragment pair at energy $E - E_0 - E_{tr}$, E_{tr}^* is the minimum E_{tr} for which $\Gamma(E_{tr},J)$ is nonzero, E_0 is the difference in zero-point energies between the unimolecular reactant and the fragment pair, $\rho_v'(E - BJ^2)$ is the vibrational density of states of the reactant at vibrational energy $E - BJ^2$, B is the geometric-mean rotational constant of the complex, and BJ^2 represents classically the rotational energy of the complex (treated as a spherical top) at angular momentum J. For tight transition states eq 15 is written as[23]

$$k^*(E,J) = \frac{G_v^*(E - E^* - B^*J^2)S}{h\rho_v'(E - BJ^2)} \tag{17}$$

where $G_v^*(E - E^* - B^*J^2)$ is the vibrational sum of states at the transition state with vibrational energy $E - E^* - B^*J^2$, E^* is the zero-point energy difference between the complex and the tight transition state, and B^* is the geometric-mean rotational constant of the transition state.

The distribution function for the energy and angular momentum of the complex formed by the thermal collision of an ion and a molecule is given by[5]

$$F(E,J) = \frac{e^{-E/kT}2J\int_{E_{tr}^*}^{E}dE_{tr}\Gamma(E_{tr},J)\rho_v(E - E_0 - E_{tr})}{\int_{E_0}^{\infty}dE\, e^{-E/kT}\int_0^{J_{max}}dJ\, 2J\int_{E_{tr}^*}^{E}dE_{tr}^*\Gamma(E_{tr},J)\rho_v(E - E_0 - E_{tr})} \tag{18}$$

where J_{max} is the maximum allowable J at a given E.

The application of eq 15–18 to the methanol system is discussed in sections IIIB, IIIC, and IIID for reactions 8, 9, and 10, respectively.

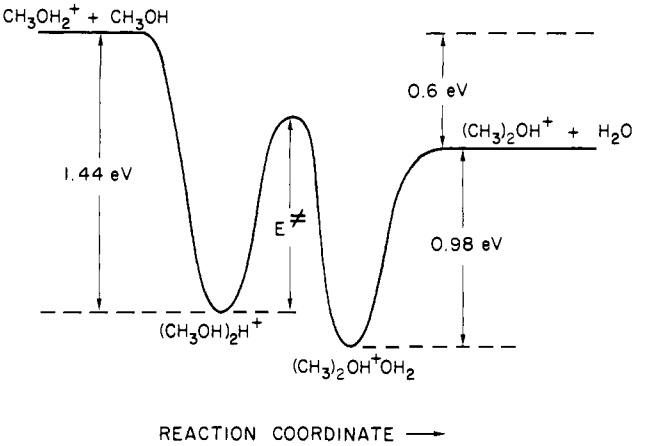

Figure 1. Schematic reaction coordinate diagram for the H_2O elimination channel used in the phase space calculations. The thermochemical data are taken from ref 27 and 28. The value of E^* is determined from theory (see text). The $(CH_3)_2OH^+OH_2$ well is present but is not used in the calculations.

B. Dimerization and Water Loss. The detailed microscopic mechanism corresponding to reaction 8 is

$$AH^+ + A \underset{k_{b1}(E,J)}{\overset{k_{f1}F_1(E,J)}{\rightleftharpoons}} [A_2H^+(E,J)]^* \tag{19a}$$

$$[A_2H^+(E,J)]^* \xrightarrow{k_{s1}[A]} A_2H^+ \tag{19b}$$

$$[A_2H^+(E,J)]^* \xrightarrow{k_{d1}(E,J)} BH^+ + H_2O \tag{19c}$$

where A = CH_3OH and B = $(CH_3)_2O$ as before. The rate constants k_{f1} and k_{s1} are calculated from ADO theory,[21] $F_1(E,J)$ is calculated from eq 18, $k_{b1}(E,J)$ is calculated from eq 16, and $k_{d1}(E,J)$ is calculated from eq 17. The parameters used in the calculations are summarized in the Appendix. The potential energy surface used is illustrated in Figure 1.

In order to use eq 11 and 12 to calculate values of k_{DIM} and k_{H_2O} for comparison with experimental data, it is first necessary to calculate phenomenological values for k_{b1} and k_{d1} by averaging the microscopic quantities $k_{b1}(E,J)$ and $k_{d1}(E,J)$, respectively, over the steady-state distribution function for $[A_2H^+(E,J)]^*$. Application of the steady-state hypothesis to the excited complex in mechanism 19 yields

$$[A_2H^+(E,J)]^* = \frac{k_{f1}F_1(E,J)[AH^+][A]}{k_{b1}(E,J) + k_{d1}(E,J) + k_{s1}[A]} \tag{20}$$

Thus, the steady-state distribution function can be written as

$$p_{ss}(E,J) = \frac{1}{N}\frac{k_{f1}F_1(E,J)}{k_{b1}(E,J) + k_{d1}(E,J) + k_{s1}[A]} \tag{21}$$

where N represents the normalization constant given by setting the integral of $p_{ss}(E,J)$ over all E and J equal to unity. The phenomenological dissociation rate constants are given by

$$k_{b1} = \int_{E_0}^{\infty}dE\int_0^{J_{max}}dJ\, k_{b1}(E,J)p_{ss}(E,J) \tag{22}$$

$$k_{d1} = \int_{E^*}^{\infty}dE\int_0^{J_{max}}dJ\, k_{d1}(E,J)p_{ss}(E,J) \tag{23}$$

The values of k_{b1} and k_{d1} calculated from eq 22 and 23, respectively, can then be used in eq 11 and 12 to predict k_{DIM} and k_{H_2O} for comparison with the experimental results.

C. Trimerization. The detailed mechanism corresponding to reaction 9 is

$$A_2H^+ + A \underset{k_{b2}(E,J)}{\overset{k_{f2}F_2(E,J)}{\rightleftharpoons}} [A_3H^+(E,J)]^* \tag{24a}$$

$$[A_3H^+(E,J)]^* \xrightarrow{k_{s2}[A]} A_3H^+ \tag{24b}$$

Step 24a cannot be treated rigorously by using the same equations

(23) (a) R. A. Marcus and O. K. Rice, *J. Phys. Colloid Chem.*, **55**, 894 (1951); G. M. Wieder and R. A. Marcus, *J. Chem. Phys.*, **37**, 1835 (1962); R. A. Marcus, *ibid.*, **20**, 359 (1952); (b) P. J. Robinson and K. A. Holbrook, "Unimolecular Reactions", Wiley-Interscience, New York, 1972; W. Forst, "Theory of Unimolecular Reactions", Academic Press, New York, 1973.

(24) H. B. Rosenstock, M. B. Wallenstein, A. L. Wahrhaftig, and H. Eyring, *Proc. Natl. Acad. Sci. U.S.A.*, **38**, 667 (1952).

(25) P. Pechukas and J. C. Light, *J. Chem. Phys.*, **42**, 3281 (1965); J. Lin and J. C. Light, *ibid.*, **43**, 3209 (1965); J. C. Light, *Discuss. Faraday Soc.*, **44**, 14 (1967); E. Nikitin, *Teor. Eksp. Khim.*, **1**, 135, 144, 428 (1965) [*Theor. Exp. Chem. (Engl. Transl.)*, **1**, 83, 90, 275 (1965)].

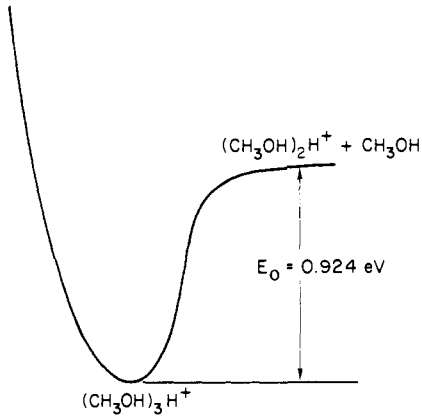

Figure 2. Schematic reaction coordinate diagram used in the phase space calculations for the formation of the proton-bound trimer in methanol.

that were used for reaction 19a because the A_2H^+ reactant in (24a) is formed via mechanism 19 and therefore is not necessarily thermalized. Any rigorous model must account in detail for all possible outcomes of the A_2H^+/A collisions in steps 19b and 24a. In both cases the initial and final states of the A_2H^+ species should be specified and some model must be used to determine if each collision results in either simple energy transfer or the formation of a long-lived complex that can be stabilized.

In the present work it is assumed that the A_2H^+ species thermalizes rotationally before reaction 24a occurs. Thus, any excess energy in the A_2H^+ reactant is vibrational. It is further assumed that all A_2H^+ ions that react in (24a) have the same amount of excess vibrational energy. Thus, the distribution function for $[A_3H^+(E,J)]^*$ formation is given by eq 18, but is shifted upward by an amount E_x, where E_x is the energy in excess of the thermal vibrational energy. Thus,

$$F_2(E,J) = F(E - E_x,J) \tag{25}$$

where $F(E - E_x,J)$ is given by eq 18 with E replaced by $E - E_x$. The rate constants k_{f2} and k_{s2} are obtained from ADO theory[21] and $k_{b2}(E,J)$ from eq 16.

Application of the steady-state hypothesis to $[A_3H^+(E,J)]^*$ in mechanism 24 yields

$$p_{ss}(E,J) = \frac{1}{N}\frac{k_{f2}F_2(E,J)}{k_{b2}(E,J) + k_{s2}[A]} \tag{26}$$

where as in eq 21 N is the normalization factor. The average rate constant for back-dissociation is

$$k_{b2} = \int_{E_0}^{\infty} dE \int_0^{J_{max}} dJ\ k_{b2}(E,J)p_{ss}(E,J) \tag{27}$$

which is substituted into eq 13 to predict values for K_{TR1} for comparison with experiment.

A summary of all the parameters used in the calculations is given in the Appendix. The potential energy surface used in the calculations is shown in Figure 2. Since no tight transition states are required, all species involved in the calculations can be characterized fairly reliably, as discussed in the Appendix. The parameter E_x is treated as an adjustable parameter. Comparisons between theory and experiment can be used to estimate the approximate range of E_x that is required for the simplified statistical model used here to yield good agreement with the experimental results.

D. Formation of the AHB^+ Dimer. The detailed mechanism corresponding to reaction 10 is

$$BH^+ + A \underset{k_{b3}(E,J)}{\overset{k_{f3}F_3(E,J)}{\rightleftharpoons}} [AHB^+(E,J)]^* \tag{27a}$$

$$[AHB^+(E,J)]^* \xrightarrow{k_{s3}[A]} AHB^+ \tag{27b}$$

$$\xrightarrow{k_{d3}(E,J)} AH^+ + B \tag{27c}$$

As with A_2H^+ in reaction 24a, the BH^+ reactant in (27a) is formed via mechanism 19 and is therefore not necessarily thermalized.

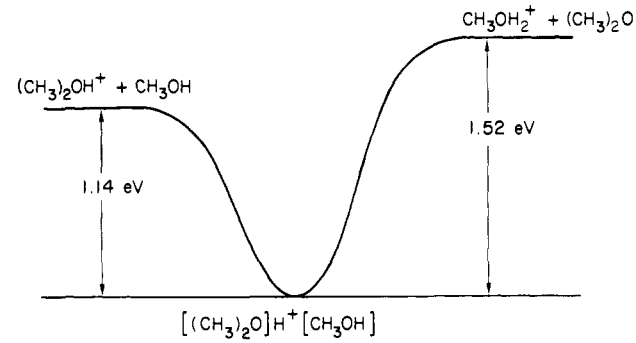

Figure 3. Schematic reaction coordinate diagram used in the phase space calculations for formation of the mixed dimethyl ether–methanol proton-bound dimer.

The same approach that was used in section IIIC to treat A_2H^+ will be used here to treat BH^+. However, it should be noted that this treatment may be a worse approximation for BH^+ than it is for A_2H^+ because BH^+ is formed by fragmentation and may, therefore, have excess translational energy as well as excess vibrational and rotational energy. If the excess translational energy is to be considered in detail then the calculation of $\Gamma(E_{tr},J)$ that is used in eq 18 must be modified to account for the excess translational energy. The treatment used here corresponds to the limiting case in which the translational excitation is small. Hence, $F_3(E,J)$ is assumed to have the same form as $F_2(E,J)$ in eq 25. ADO theory[21] is used to estimate k_{f3} and k_{s3}. Reactions 27a and 27c are both assumed to be governed by orbiting transition states. Hence, $k_{b3}(E,J)$ and $k_{d3}(E,J)$ are both given by eq 16.

The steady-state distribution function for $[AHB^+(E,J)]^*$ is

$$p_{ss}(E,J) = \frac{1}{N}\frac{k_{f3}F_3(E,J)}{k_{b3}(E,J) + k_{d3}(E,J) + k_{s3}[A]} \tag{28}$$

and the average rate constants for dissociation are

$$k_{b3} = \int_{E_0}^{E} dE \int_0^{J_{max}} dJ\ k_{b3}(E,J)p_{ss}(E,J) \tag{29}$$

$$k_{d3} = \int_{E_0}^{E} dE \int_0^{J_{max}} dJ\ k_{d3}(E,J)p_{ss}(E,J) \tag{30}$$

The values of k_{b3} and k_{d3} obtained in eq 29 and 30, respectively, are used in (14) to predict values of k_{AHB} for comparison with experimental data.

The potential energy surface used in the calculations is shown in Figure 3. The parameters used in the calculations are summarized in the Appendix.

IV. Results

A. Rate Constants. The primary data are second-order rate constants for the four phenomenological reactions 4 to 7. Only reaction 5 is a true bimolecular process. Reactions 4, 6, and 7 are association reactions, and hence the second-order rate constants should be pressure dependent in the low-pressure regime. These reactions should also exhibit a substantial temperature dependence.

In Figure 4, the apparent second-order rate constant k_{DIM} for reaction 4 is plotted as a function of pressure ($(1–10) \times 10^{-4}$ torr) for T = 295 K. As expected, the value of k_{DIM} increases nearly linearly with pressure over this range. The data shown are typical of a number of data sets taken at this temperature. The variation in the data sets was usually less than 30% and always showed approximately the same pressure dependence. This uncertainty is not unexpected for rate constants in the 10^{-12} or low 10^{-11} cm^3/s range for a "sticky" substance like methanol. The solid line is a theoretical fit to the data. Comments on this fit will be reserved for the Discussion section.

Figure 5 gives the variation in k_{DIM} with temperature (220–360 K) for a constant pressure of 5×10^{-4} torr. Clearly a strong negative temperature dependence is evident. If one assumes a temperature dependence of the form[26]

$$k = CT^m \tag{31}$$

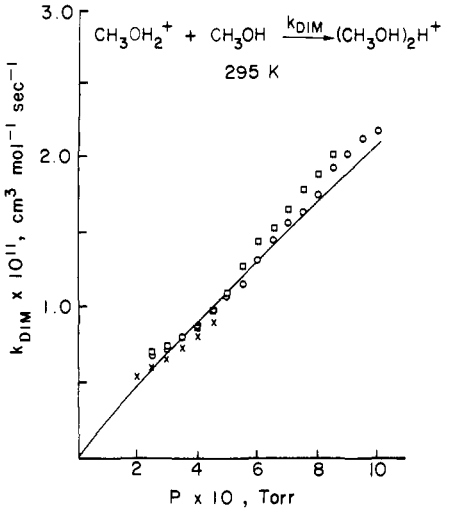

Figure 4. A plot of k_{DIM} vs. pressure at 295 K. The uncertainty is ±30%. The line is a theoretical calculation (see text).

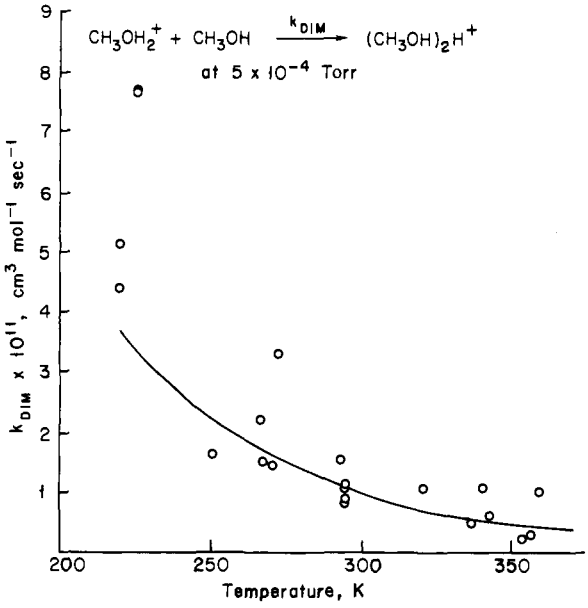

Figure 5. A plot of k_{DIM} vs. temperature at 5 × 10^{-4} torr. The line is a theoretical calculation (see text).

where C and m are constants, then a plot of log T vs. log k has a slope of $m = 4.6 \pm 1.2$. There is substantial scatter in the data, of the order of ±30%. The solid line is the theoretical fit using the same parameters that were used in Figure 4.

The rate constant for reaction 5, H_2O elimination, is $9 \pm 3 \times 10^{-11}$ cm^3/s at 300 K independent of pressure. This lack of pressure dependence is expected for a purely second-order reaction. It is also evidence that the internal energy in the reactant $CH_3OH_2^+$ ions does not vary with pressure, indicating a near thermal energy distribution for these ions in our experiments. The temperature dependence of reaction 5 is given in Figure 6. A clear negative temperature dependence is observed, with $m = -2.77 \pm 0.3$. The solid line is a theoretical curve using the same parameters as those given in Figures 4 and 5.

The pressure dependence of the apparent second-order rate constant, k_{TRI}, for the trimerization reaction 6 is given in Figure 7 over the range (3–10) × 10^{-4} torr at 295 K. These data are typical and separate runs on other days were within ±30%. A substantial, near linear, increase in k_{TRI} is observed. Two theoretical lines are given. One of them is based on the assumption that the $(CH_3OH)_2H^+$ dimer has no excess internal (vibrational) energy and the second on the assumption that the dimer has an

(26) D. R. Bates, *J. Phys. B*, **12**, 4135 (1979).

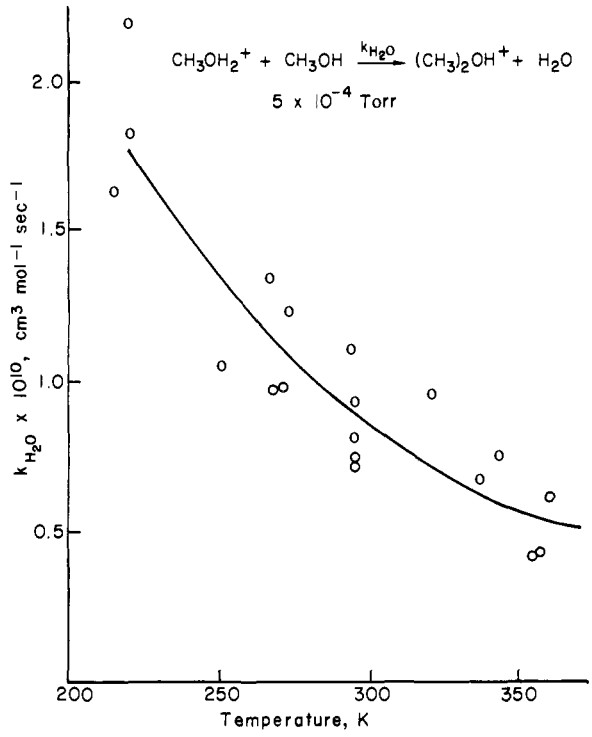

Figure 6. A plot of k_{H_2O} vs. temperature at 5 × 10^{-4} torr. The line is a theoretical calculation (see text).

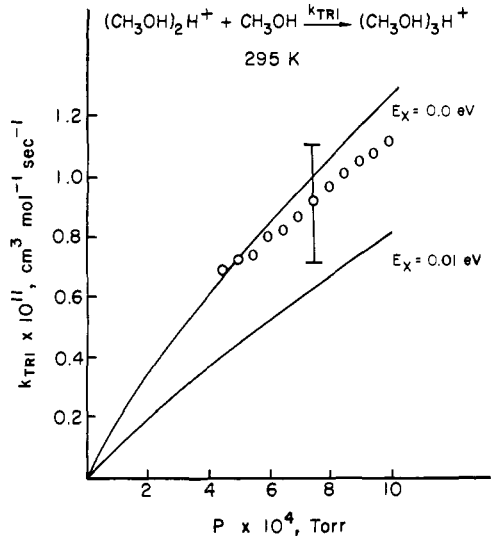

Figure 7. A plot of k_{TRI} vs. pressure at 295 K. The two lines are theoretical calculations, where E_x is the excess vibrational energy in $(CH_3OH)_2H^+$ (see text). The experimental uncertainty is ±30%.

excess internal energy of 0.01 eV. The dramatic dependence of k_{TRI} on excess internal energy is evident.

Figure 8 presents the temperature dependence of k_{TRI} at 5 × 10^{-4} torr pressure. The range is small, $220 \leq T \leq 295$ K, due to low signal to noise at higher temperatures. The temperature coefficient can only be crudely estimated as $m \simeq 6 \pm 2$. Three theoretical lines are given for excess energies of 0, 0.01, and 0.02 eV. The parameters used are the same as those that generated the theoretical line in Figure 7.

The dependence of the apparent second-order mixed dimer association rate constant, k_{AHB}, on pressure is given in Figure 9 for $T = 295$ K. The expected near linear increase of k_{AHB} with pressure is apparent. Three theoretical curves are also given, assuming excess internal energies of 0.03, 0.35, and 0.04 eV. The theoretical curve for 0 eV excess internal energy predicts k_{AHB} will increase with pressure very much faster than experimentally observed.

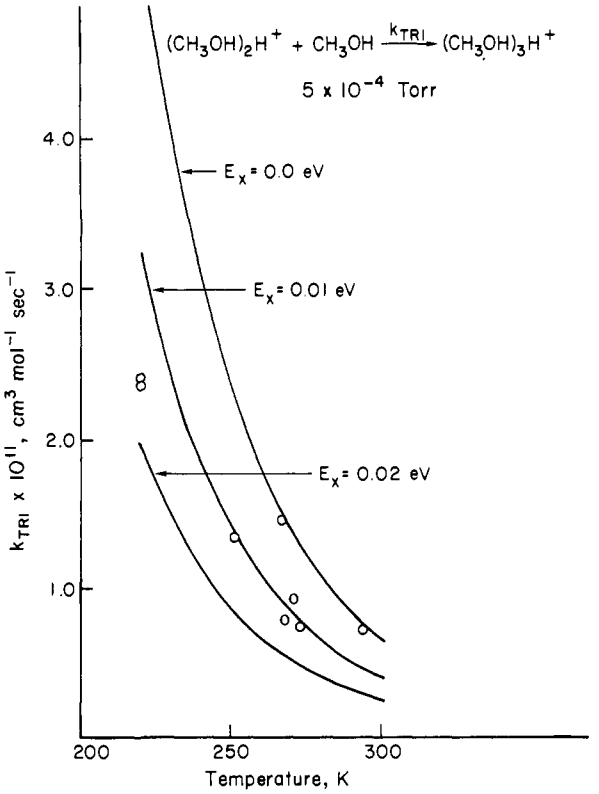

Figure 8. A plot of k_{TRI} vs. temperature at 5×10^{-4} torr. The three lines are theoretical calculations where E_x is the excess vibrational energy in $(CH_3OH)_2H^+$ (see text).

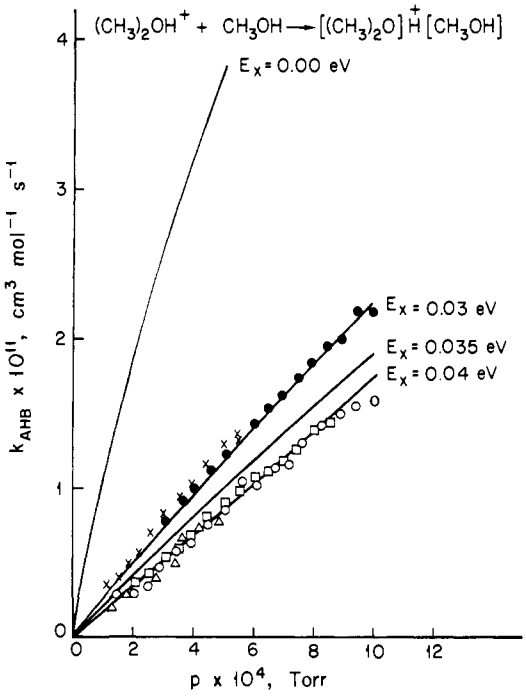

Figure 9. A plot of k_{AHB} vs. pressure at 295 K. The four lines are theoretical calculations, where E_x is the excess vibrational energy in $(CH_3)_2OH^+$ (see text).

The variation of k_{AHB} with temperature is given in Figure 10 for $p = 5 \times 10^{-4}$ torr. As expected, the clustering reaction shows a strong negative temperature dependence, $m = 5.4 \pm 1.5$. Again three theoretical curves are given for excess energies of 0.03, 0.035, and 0.04 eV. The same parameters were used for these curves as for those in Figure 9.

A summary of the temperature coefficients of these reactions as well as the theoretical predictions of the phase space theory

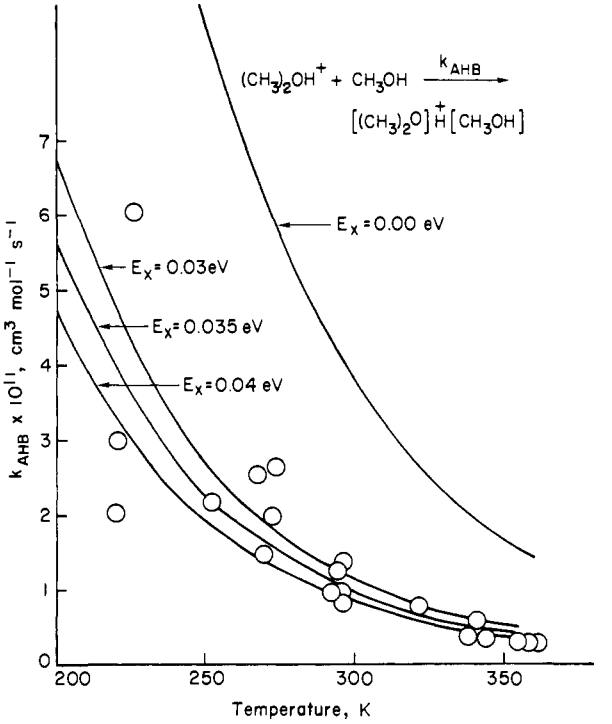

Figure 10. A plot of k_{AHB} vs. temperature at 5×10^{-4} torr. The four lines are theoretical calculations, where E_x is the excess vibrational energy in $(CH_3)_2OH^+$ (see text).

Table I. Comparison of the Temperature Dependence of Association Rate Constants with Theory[d]

reaction	expt[a]	theory: phase space[b]	theory: Bates[c]
$CH_3OH_2^+ + CH_3OH \rightarrow (CH_3OH)_2H^+$	-4.6 ± 1.2	−4.45	$-(3 + \delta)$
$(CH_3OH)_2H^+ + CH_3OH \rightarrow (CH_3OH)_3H^+$	-6 ± 2	−6.5	$-(3 + \delta)$
$(CH_3)_2OH^+ + CH_3OH \rightarrow [(CH_3)_2O]H^+[CH_3OH]$	-5.4 ± 1.5	−4.8	$-(3 + \delta)$
$CH_3OH_2^+ + CH_3OH \rightarrow (CH_3)_2OH^+ + H_2O$	-2.7 ± 0.3	−2.5	

[a] This work. [b] This work. The phase space results do not rigorously fit a power law temperature dependence. The actual phase space temperature dependence is given in Figures 5, 6, 8, and 10. The numbers in the table are for comparison purposes only. [c] D. R. Bates, ref 26. The factor δ has to do with stabilization efficiency. [d] The form $k = CT^m$ is assumed for convenience in the comparison, where m is listed in the table.

described here and the canonical theory of Bates[26] is given in Table I. It should be noted that the phase space theory does not rigorously predict a power law dependence of k on T for association reactions. However, for the limited temperature range of these experiments such a dependence roughly holds. The intent of Table I is to allow comparisons between the two theories as well as experiment. The best comparison between phase space theory and experiment is given in Figures 4–10, however.

B. Kinetic Energy Distribution. The proton bound dimer of methanol can be formed in the ion source of the V. G. Analytical ZAB-2F mass spectrometer, extracted, mass selected, and allowed to undergo unimolecular decomposition in the second field free region. The metastable for the water loss process

$$[(CH_3OH)_2H^+]^* \rightarrow (CH_3)_2OH^+ + H_2O \qquad (32)$$

has been observed and the kinetic energy distribution obtained by using methods previously described.[19] The average kinetic energy release is 75 meV as determined from the distribution. The results are given in Figure 11.

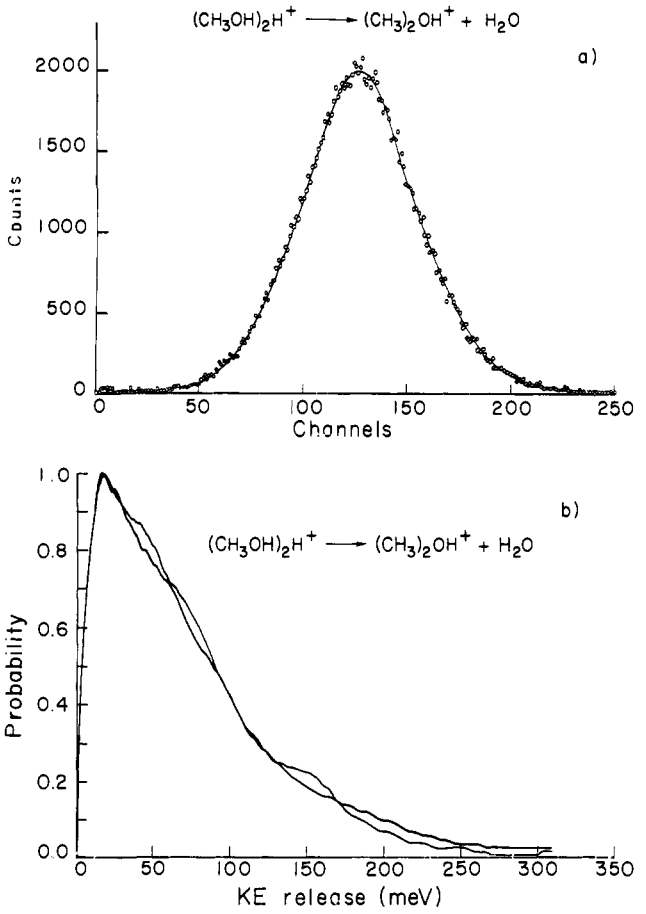

Figure 11. (a) The metastable peak shape for formation of $(CH_3)_2OH^+$ from the proton-bound dimer of methanol. The points are taken from individual channels on a multichannel analyzer and the solid line is a computer-smoothed fit to the points. (b) A plot of relative probability vs. kinetic energy release of the metastable peak in part a. The two curves are obtained from the two halves of the metastable peak. The computer-smoothed curve in part a was used to obtain the distributions.

V. Discussion

It is convenient to separate the discussion into several parts. The reaction system has been treated as three separate systems theoretically and these will be discussed separately. An additional section will separately discuss quantitative aspects of the temperature dependence of the association reactions.

A. Reaction of $CH_3OH_2^+$ with CH_3OH. The reaction system is summarized in eq 8. The first question that had to be addressed in modeling the reactions was the nature of the transition state in the water loss channel 9b. If this channel is assumed to have an orbiting transition state, then theory predicts that this channel should dominate at all temperatures and pressures reported here. As a result, k_{H_2O} should equal the collision rate and exhibit only a very weak temperature dependence. In fact, k_{H_2O} is significantly smaller than the collision rate ($k_{H_2O}/k_{collision} \simeq 0.05$) and hence a tight transition state must dominate this channel. Consequently it is necessary to specify transition-state properties, including energy $E^\ddagger$, mean rotational constant $B^\ddagger$, and vibrational frequencies. The vibrational frequencies were chosen on a rational basis (Appendix) and were not varied. It was found that reasonable agreement between experiment and theory could be obtained for the range of values $1.05\ \text{eV} \le E^\ddagger \le 1.20\ \text{eV}$ (see Figure 1) and $0.1\ \text{cm}^{-1} \le B^\ddagger \le 0.22\ \text{cm}^{-1}$. The range of $B^\ddagger$ is determined in part by the requirement that the transition-state structure be physically reasonable. It was decided to choose values in the middle of each range for the final calculations reported in Figures 4–6: $E^\ddagger = 1.15$ eV and $B^\ddagger = 0.15\ \text{cm}^{-1}$.

A word should be said about the potential surface drawn in Figure 1. First, two deep wells are present; the first corresponding to the proton-bound dimer of CH_3OH and the second to the proton-bound dimer of $(CH_3)_2O^+/H_2O$. The well depths have been measured by Hiraoka et al.[27a] and Grimsrud and Kebarle[27b] and the relative assymptotic energy values for $CH_3OH_2^+/CH_3OH$ and $(CH_3)_2OH^+/H_2O$ taken from literature data.[28] We assume the energy barrier for H_2O elimination separates these two wells and does not exist in the exit channel for $(CH_3)_2OH^+/H_2O$ formation. This assumption is consistent with the fact that $(CH_3)OH^+$ associates with water with no apparent barrier.[27]

The kinetic energy distribution in Figure 11b is derived from a metastable transition and hence corresponds to dissociation of $(CH_3OH)_2H^+$ ions with lifetimes in the 1 to 10 μs time scale. The experiments were performed under conditions where the $(CH_3OH)_2H^+$ ions probably had not undergone any stabilizing collisions and thus would have internal energies of $\sim$0.3 eV above the energy of the tight transition state predicted from the kinetic studies. $(CH_3OH)_2H^+$ ions in this energy range could have isomerization lifetimes of 10^5–$10^6\ \text{s}^{-1}$ as required for the metastable. The fact that the experimental kinetic energy distribution for $(CH_3)_2OH^+/H_2O$ formation peaks at $\sim$0.025 eV suggests most of the total available energy, $\sim$0.6 eV (see Figure 1), ends up as internal energy in the products. Unfortunately we are not yet able to calculate a kinetic energy distribution for reaction coordinates as complex as that of Figure 1, and hence we cannot compare theory with experiment in this case.

The predictions of the theoretical model are compared with the kinetic experimental results in Figures 4–6. In general, the agreement is very good although the scatter in the experimental data prevents precise comparisons. It appears that the rate constant for the association reaction, k_{DIM}, increases faster at low temperature than predicted by theory. The overall dependence is well produced, however.

The bimolecular rate constant k_{H_2O} has a fairly strong negative temperature dependence (Figure 6), a dependence that is accurately reproduced by theory. The negative temperature dependence results from the fact that the sum of states at the tight transition state for H_2O loss (see Figure 1) increases less rapidly than the sum of states in the orbiting transition state for $CH_3OH_2^+/CH_3OH$ formation as temperature increases.[29] This negative temperature dependence is also strong evidence that the tight transition state regulates the H_2O loss channel. An orbiting transition state such as that in the $(CH_3)OH^+/H_2O$ exit channel would result in little or no temperature dependence.

Kleingeld and Nibbering[30] have recently reported some interesting work on this system. They studied reaction 32

$$CH_3{}^{18}OH^+{}_2 + CH_3{}^{16}OH \rightarrow \begin{cases} (CH_3)_2{}^{16}OH^+ + H_2{}^{18}O & \text{(32a)} \\ (CH_3)_2{}^{18}OH^+ + H_2{}^{16}O & \text{(32b)} \end{cases}$$

and determined that $k(32a)/k(32b) \simeq 3/1$ where the statistical distribution is 1/1. This is a surprising result since it seemingly rules out a long-lived complex of type I. Kleingeld and Nibbering

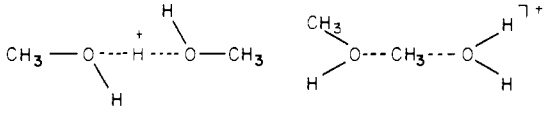

I II

suggest an intermediate of type II. A third possibility is the dimethyl ether–water proton-bound dimer III, where the oxygen in the water moiety would come predominantly from the protonated methanol collision partner. Hiraoka et al.[27a] have shown

(27) (a) K. Hiraoka, E. P. Grimsrud, and P. Kebarle, *J. Am. Chem. Soc.*, **96**, 3359 (1974). (b) E. P. Grimsrud and P. Kebarle, *ibid.*, **95**, 7939 (1973).

(28) D. H. Aue and M. T. Bowers in "Gas Phase Ion Chemistry", Vol. 2, M. T. Bowers, Ed., Academic Press, New York, 1979, pp 2–52.

(29) W. E. Farneth and J. I. Brauman, *J. Am. Chem. Soc.*, **98**, 7891 (1976); W. N. Olmstead and J. I. Brauman, *ibid.*, **99**, 4219 (1977). These authors did not actually discuss the temperature dependence of reactions, but the ideas basic to the interpretation given here were first elucidated in these works.

(30) J. C. Kleingeld and N. M. M. Nibbering, *Org. Mass Spectrom.*, **17**, 136 (1982).

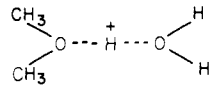

III

that III is stable to dissociation to $(CH_3)_2OH^+$ and H_2O by 22.6 kcal/mol (0.98 eV). However, structure III is unlikely in view of recent experiments of Kebarle to be discussed shortly.

In contrast to the findings of Kleingeld and Nibbering,[30] our kinetic results have all been nicely explained by invoking structure I as the initial $C_2H_9O_2^+$ intermediate. Support for this structure comes from recent work of Kebarle.[30] He reports that in a mixture of 0.1 torr of CH_3OH and 2 torr of CH_4 the *only* species observed in the first millisecond of reaction time are $(CH_3OH)_nH^+$ clusters with n = 2–5. There are *no* clusters containing $(CH_3)_2O$ or H_2O, indicating at 2 torr of total pressure all $CH_3OH_2^+$ reacts with CH_3OH to form methanol clusters only. Hence, all $CH_3OH_2^+$ ions sample structure I in Kebarle's experiment in agreement with our interpretation. The results of Kleingeld and Nibbering are thus anomalous. The possibility exists that Kleingeld and Nibbering are dealing with internally excited $CH_3OH_2^+$ ions, and these excited ions could directly react via struture II. There is no evidence for this explanation, however, and at this time the reason for the disparity between our results and Kebarle's result, and Kleingeld and Nibbering's result, must remain unanswered.

B. Reaction of $(CH_3OH)_2H^+$ with CH_3OH. The reaction scheme is given in eq 9, and is essentially the same as that used to successfully explain clustering of protonated amines.[4-7] The one difference is the $(CH_3OH)_2H^+$ reactant ion is itself the product of association of $CH_3OH_2^+$ with CH_3OH_2. As a consequence there may be some residual internal energy in $(CH_3OH)_2H^+$ that will manifest itself in the association rate constant. Ideally an energy-transfer mechanism would be built into the kinetic scheme to account for this effect. As a first step we have assumed that $(CH_3OH)_2H^+$ is rotationally and translationally thermalized but may retain some vibrational internal energy, E_x. Other than that difference, all of the usual assumptions of phase space theory are invoked. The results for several values of E_x are given in Figures 7 and 8. From comparison of experiment and theory it appears that $(CH_3OH)_2H^+$ clusters may retain some internal energy, but on the average it is probably not much larger than 0.01 eV. From these calculations it is clear that k_{TR1} is extremely sensitive to internal energy. For example, adding just 0.01 eV of internal energy in $(CH_3OH)_2H^+$ decreases k_{TR1} by 60%. Such large changes are easily detectable even with experiments in which the uncertainty is ±30%. A further comment will be made in section VC. It appears the trimerization reaction in methanol is nicely fit by using the statistical model developed in section III.

C. Reaction of $(CH_3)_2OH^+$ with CH_3OH. The reaction scheme for this system is given by eq 10. Reaction 10b is endothermic by 7.6 kcal/mol and should not be an important factor. The $(CH_3)_2OH^+$ ion is formed by reaction sequence 8 and can be translationally, rotationally, and vibrationally excited. In the calculations it was assumed that $(CH_3)_2OH^+$ was translationally and rotationally thermalized but might contain excess vibrational energy. In Figures 9 and 10 calculations are reported for E_x = 0, 0.03, 0.035, and 0.04 eV. It is apparent that calculated values of k_{AHB} increase with pressure much faster than experiment for E_x = 0 (Figure 9). Similar results are found for the variation of k_{AHB} with temperature (Figure 10), where k_{AHB} increases with decreasing temperature for E_x = 0 much faster than experiment. An average value of E_x = 0.035 ± 0.005 fits the data. Again the strong dependence of k_{AHB} on E_x is apparent and there can be little doubt $(CH_3)_2OH^+$ ions that associate with CH_3OH are vibrationally excited. Internal excitation in $(CH_3)_2OH^+$ is consistent with the kinetic energy distribution for formation of this ion as discussed in section VA.

These two systems, characterized by k_{TR1} and k_{AHB}, are the only two in which the effect of internal energy has been explored for clustering reactions. The present theoretical model of simply adding an extra amount of vibrational energy to the reactant ion is easy to accomplish theoretically and has the virtue of adequately

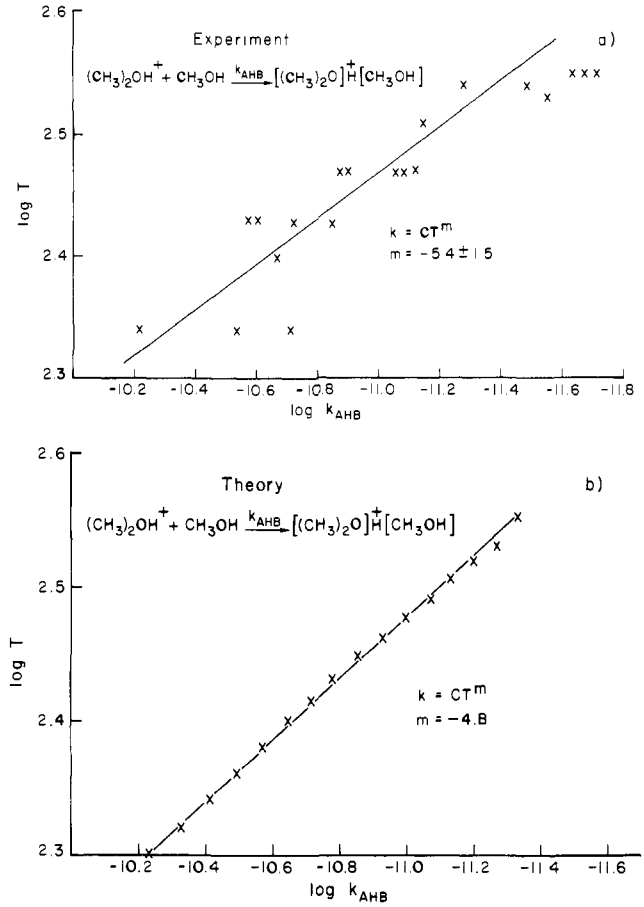

Figure 12. (a) A plot of log T vs. log k_{AHB} for experimental points in Figure 10. (b) A plot of log T vs. log k_{AHB} for the theoretical line in Figure 10.

fitting the experimental data. It is not satisfactory from the perspective that E_x must be treated as a variable parameter with no a priori basis. It is very desirable to extend the theoretical model to include explicitly an energy-transfer mechanism, both to investigate the efficiency of energy removal/addition by collisions and to provide a basis for simplifications of the type employed here. It is probable that as higher order clustering is studied, larger amounts of internal energy will be stored in the reactant ions. Some plausable theoretical method of dealing with this phenomena is necessary if a quantitative clustering/nucleation model is to be developed.

D. Temperature Dependence. The temperature dependence of the clustering rate constants is given in Figures 5, 8, and 10. In the ICR the pressures are low enough that to a good approximation the systems are in the low pressure limit. This assumption is supported by the fact that k_{DIM}, k_{TR1}, and k_{AHB} all increase essentially linearly with pressure. If these three rate constants are assumed to follow a power law dependence on temperature, as given by eq 31, then a plot of log k vs. log T should give a straight line with slope m. An example is given in Figure 12 for the $(CH_3)_2OH^+/CH_3OH$ association reaction. The phase space theory obeys rather closely the assumed power law dependence. Experiment seems to show some curvature in the log k_{AHB} vs. log T plot, but the scatter is such one cannot say for sure.

The theory of Bates[26] suggests a power law dependence of k on T should be observed in the low pressure limit. If one ignores the temperature dependence of the stabilization step (as is done in the phase space theory approach presented here), the theory of Bates indicates $m = l/2$, where l is the total number of rotational degrees of freedom of the reactants. Hence, for two polyatomic molecules as we have here, l = 6 and m = −3. Bates suggests this dependence might need to be augmented by the temperature dependence of the collisional stabilization step. Empirically, then the dependence would be $m = -l/2 - \delta$ where

Table II. Parameters Used for Neutral Species

	$(CH_3)_2O$	CH_3OH	H_2O
ν_i[a]	3000 (4)	3700	3750
	2800 (2)	3000	3650
	1460 (6)	2950	1600
	1240	2850	
	1230	1470 (3)	
	1180	1350	
	1150	1170	
	1100	1060	
	930	1030	
	420	250	
	240		
	200		
B[b]	0.441	1.39	16.08
σ[c]	2	1	2

[a] Vibrational frequencies in cm^{-1} (degeneracy in parentheses). [b] Geometric-mean rotational constant in cm^{-1}. [c] Symmetry number.

δ is a factor that varies from system to system. If you assume[26] the stabilization efficiency varies with the energy above the dissociation limit, ϵ, with functional form $a\epsilon^u e^{-\epsilon/k\theta}$, where a, u, and θ are constants, then it turns out $\delta \geq {}^3/_2$. Such a dependence would bring the theory of Bates into approximate agreement with the experimental data reported here. It seems difficult to rationalize a stabilization efficiency with such a strong energy dependence for colliders as large as CH_3OH. It also seems unnecessary to invoke this temperature dependence since the phase space theory can explain both the pressure dependence and the temperature dependence of k_{DIM}, k_{TRI}, and k_{AHB} assuming unit stabilization efficiency independent of temperature. This is still an open question, however, and neither the data nor theoretical model presented here are of high enough quality to fully resolve it.

VI. Conclusions

1. A phase space form of statistical rate theory is applied to clustering reactions of $CH_3OH_2^+$, $(CH_3)_2OH^+$, and $(CH_3OH)_2H^+$ with CH_3OH. In all cases both the pressure and temperature dependence of the rate constants are adequately modeled by theory.

2. In the reaction of $CH_3OH_2^+$ with CH_3OH formation of $(CH_3)_2OH^+$ and H_2O completes with clustering. The fact that this channel proceeds at only 5% of the collision rate and the fact that it has a strong negative temperature dependence require a tight transition state dominate the rate for H_2O elimination. Theoretical modeling suggests a barrier of 0.17 ± 0.1 eV relative to $(CH_3)_2OH^+/H_2O$ at infinite separation. The mechanism of this reaction is not yet understood, however, as recent measurements by Kleingeld and Nibbering indicate the oxygen atom in the H_2O products may come preferentially from the $CH_3OH_2^+$ reactant. These experiments are at odds, however, with recent results of Kebarle that agree with our assumption of a proton-bound dimer of CH_3OH as the key intermediate.

3. Both $(CH_3OH)_2H^+$ and $(CH_3)_2OH^+$ appear to have small amounts of residual vibration energy when they form clusters with lifetimes on the ICR time scale ($\tau > 10^{-4}$ s). The phase space theory successfully models the experimental data assuming $(CH_3OH)_2H^+$ has ~0.01 eV of vibrational energy and $(CH_3)_2OH^+$ has ~0.035 eV of vibrational energy. Both rotational and translational energies are assumed thermal. The need for a realistic energy-transfer mechanism is emphasized.

4. The negative temperature dependence of the association reactions could be approximately modeled with a power law dependence on temperature. Exponent values in the range $m = -4$ to -6 were observed. The phase space theory yields a near power law dependence over the limited temperature range reported, with exponent values in good agreement with theory. The phase space theory assumed the stabilization efficiency was unity and independent of temperature. A canonical theory of Bates[26] yields a temperature dependence of $m = -3$ if the stabilization step is assumed independent of temperature. Better agreement of Bates theory with experiment is obtained if a temperature dependence of the stabilization step is assumed.

Table III. Parameters Used for Protonated Species

	$(CH_3)_2OH^+$		$CH_3OH_2^+$	
ν_i[a]	3700	1180	3700 (2)	1350
	3000 (4)	1150	3000	1170
	2800 (2)	1100	2950	1060
	1460 (6)	930	2850	1030
	1350 (2)	420	1600 (2)	250
	1240	240	1470 (3)	
	1230	200		
B[b]	0.410		1.23	
σ[c]	2		1	

[a] Vibrational frequencies in cm^{-1} (degeneracy in parentheses). [b] Geometric-mean rotational constant in cm^{-1}. [c] Symmetry number.

Table IV. Parameters Used for Proton-Bound Polymers

	$(CH_3OH)_2H^+$	$(CH_3OH)_3H^+$	$[CH_3OH][(CH_3)_2O]H^+$	
ν_i[a]	3700 (2)	3700 (3)	3700	1150
	3000 (2)	3000 (3)	3000 (5)	1100
	2950 (2)	2950 (3)	2950	1060
	2850 (2)	2850 (3)	2850	1030
	1670	1670 (2)	2800 (2)	930
	1470 (6)	1470 (9)	1660	440
	1350 (4)	1350 (6)	1470 (3)	420
	1170 (2)	1170 (3)	1460 (6)	250
	1060 (2)	1060 (3)	1350 (2)	240
	1030 (2)	1030 (3)	1240	200
	490	490	1230	180 (3)
	300 (2)	250 (3)	1180	100 (2)
	250 (2)	140 (3)	1170	
	100 (2)	100 (3)		
B[b]	0.130	0.072	0.098	
σ[c]	2	3	1	
B_{int}[d]	1.18	1.07 (3)	1.24	
σ_{int}[e]	1	1	1	

[a] Vibrational frequencies in cm^{-1} (degeneracy in parentheses). [b] Geometric-mean rotational constant in cm^{-1}. [c] Symmetry number. [d] Rotational constant for internal rotor, in cm^{-1} (degeneracy in parentheses). [e] Symmetry number for internal rotor.

Table V. Parameters Used for the Tight Transition State for $(CH_3OH)_2H^+ \rightarrow (CH_3)_2OH^+ + H_2O$

ν_i[a]	3700 (2)	500 (2)
	2950 (6)	350 (2)
	1400 (4)	250
	1200 (4)	200
	1000 (4)	100 (2)
	800 (4)	
B[b]	0.150	
σ[c]	1	
$E^{\ddagger}$[d]	1.150	

[a] Vibrational frequencies in cm^{-1} (degeneracy in parentheses). [b] Geometric-mean rotational constant in cm^{-1}. [c] Symmetry number. [d] Barrier height in eV (see Figure 1).

Acknowledgment. We gratefully acknowledge the National Science Foundation under Grant CHE80-20464 and the donors of the Petroleum Research Fund, administered by the American Chemical Society, for support of this research. We also wish to thank Professor Paul Kebarle for a very useful and thoughtful review of the manuscript and for communicating unpublished results to us on clustering of $CH_3OH_2^+$ with CH_3OH.

VII. Appendix. Parameters Used in Phase Space Calculations

Neutral Species. Literature values are used for all the vibrational frequencies in methanol, dimethyl ether, and water,[31] and

(31) T. Shimanouchi, "Tables of Molecular Vibrational Frequencies", Consolidated Vol. I, National Bureau of Standards, Washington, D.C., 1972.

for the rotational constant of water.[32] The rotational constants for methanol and dimethyl ether are calculated from the structures assuming that bond angles about carbon and oxygen are tetrahedral and using bond lengths (in Å) of 0.956 for O–H, 1.43 for C–O, and 1.10 for C–H.[33] The final set of parameters used for these species is summarized in Table II.

Protonated Species. Vibrational frequencies for $CH_3OH_2^+$ and $(CH_3)_2OH^+$ are taken to be those of the nonprotonated neutrals with three additional frequencies added to account for the proton (one stretch and two bends). Rotational constants are calculated from the structures assuming 120° bond angles (planar) about oxygen[34] and taking the O–H bond length to be 1.0 Å, and assuming that the rest of the structure is the same as that of CH_3 neutral. The final parameters used are summarized in Table III.

Proton-Bound Polymers. There are three polymers to consider: $(CH_3OH)_2H^+$, $(CH_3OH)_3H^+$, and $[CH_3OH][(CH_3)_2O]H^+$. In each case it is assumed that each of the neutral ligands retains its vibrational frequencies in the polymer. Each of the dimers has one internal rotation, and the trimer has three internal rotations for which the rotational constants can be calculated from the structures. This leaves nine vibrational modes in each dimer and twelve vibrational modes in the trimer for which the frequencies are not well known. Some of these can be estimated by comparison with other species, but for some modes it is difficult to obtain any reliable estimate of the frequencies. These are chosen so that the resulting value of ΔS calculated from statistical thermodynamics for the association reaction of interest agrees with the experimental value.[27b] Rotational constants for the polymers are calculated by assuming that the bond angles about oxygen are 120° and that the O–H^+–O bond angles are 180° in the dimers and 120° in the timer, and taking the O–H^+ bond lengths to be 1.2 Å. The parameters are summarized in Table IV.

Transition States. There are three orbiting transition states to consider: $CH_3OH_2^+ + CH_3OH$; $(CH_3OH)_2H^+ + CH_3OH$; and $(CH_3)_2OH^+ + CH_3OH$. In each case the parameters for the separated fragments are obtained as explained above for each species. The zero-point energy differences, E_0, as shown in Figures 1 to 3, are taken to be equal to the ΔH values, which are available in the literature.[27b]

The only tight transition state in this work is that for water loss from the proton-bound methanol dimer. The structure and properties of this transition state are essentially unknown, as discussed in the text. Regardless of the exact structure, a number of vibrational frequencies can be estimated from those of the methyl group and methanol molecule. The remaining frequencies, as well as the rotational constant and energy barrier, $E^{\ddagger}$, as shown in Figure 1, must be treated here as adjustable parameters. The final set of parameters used in the calculations is summarized in Table V.

Registry No. $CH_3OH_2^+$, 17836-08-7; $(CH_3)_2OH^+$, 17009-82-4; CH_3OH, 67-56-1.

(32) G. Herzberg, "Molecular Spectra and Molecular Structure", Vol. III, Van Nostrand, Princeton, N.J., 1967.
(33) R. C. Weast, (Ed., "Handbook of Chemistry and Physics", Chemical Rubber Co., Cleveland, Ohio, 1979.
(34) L. M. Tel, S. Wolfe, and I. G. Csizmadia, *J. Chem. Phys.*, **59**, 4047 (1973).

Nature of the Frontier Orbitals in Phosphine, Trimethylphosphine, and Trifluorophosphine

Shen-Xiu Xiao,[†] William C. Trogler,*[‡] D. E. Ellis,* and Ziva Berkovitch-Yellin[§]

Contribution from the Department of Chemistry, Northwestern University, Evanston, Illinois 60201. *Received March 14, 1983*

Abstract: The electronic structures of PH_3, $P(CH_3)_3$, and PF_3 have been examined with the aid of self-consistent multipolar Xα calculations (SCM-Xα-DV). There is excellent agreement between the theoretical and experimental ionization energies. When the transition-state procedure is used, first ionization potentials of 10.39, 8.41, and 12.19 eV are calculated for PH_3, $P(CH_3)_3$, and PF_3, respectively. Experimental values are 10.58, 8.58, and 12.27 eV, respectively. Plots of the highest and lowest unoccupied orbitals provide insight into the role of phosphorus donor ligands in transition-metal systems. Especially interesting is the π-symmetry p–d hybrid that comprises the lowest empty orbital in the π-acceptor PF_3 ligand.

Trivalent phosphorus donor ligands, PZ_3 (Z = F, Cl, H, alkyl, aryl, *O*-alkyl, *O*-aryl), have played an important role in the development of coordination and organometallic chemistry. They form tractable complexes with nearly all the transition elements, and PZ_3 ligands are compatible with most metal oxidation states and ancillary ligands. The electron-pair donor properties of phosphine ligands appear to follow sensible patterns. For example, trialkylphosphines generally form stronger metal–ligand bonds than triarylphosphines, when ligand basicity effects predominate.[1] Of course, steric factors[2] may be important in congested complexes. Ligand basicity trends fail to explain[3] the unusual stability of complexes that contain phosphite and PX_3 (X = F, Cl) ligands. Because these latter compounds frequently contain metals in low formal oxidation states, it has been generally thought that π-acceptor behavior may be important; however, arguments[3-11] can be made either in favor or against the π acidity of the PZ_3 ligand. Our interest centers around the following question; if PZ_3 ligands exhibit π-acceptor properties, then what is the nature of the

[†] Permanent address: Department of Chemistry, Sichuan University, Chengdu, Sichuan, Peoples Republic of China.
[‡] Alfred P. Sloan Research Fellow (1983–1985). After September, 1983, address correspondence to this author at the Department of Chemistry D-006, University of California, San Diego, La Jolla, CA 92093.
[§] Permanent address: Department of Structural Chemistry, Weizmann Institute of Science, Rehovot, Israel.

(1) Tolman, C. A. *J. Am. Chem. Soc.* **1970**, *92*, 2953–2956.
(2) Tolman, C. A. *Chem. Rev.* **1977**, 77, 313–348.
(3) Huheey, J. E. "Inorganic Chemistry: Principles of Structure and Reactivity"; Harper & Row: New York, 1972; pp 350–358.
(4) Basolo, F.; Pearson, R. G. "Mechanisms of Inorganic Reactions"; John Wiley and Sons, Inc.: New York, 1967; pp 527–540.
(5) Mason, R.; Meek, D. W. *Angew. Chem., Int. Ed. Engl.* **1978**, *17*, 183–194.
(6) Yarbrough, L. W.; Hall, M. B. *Inorg. Chem.* **1978**, *17*, 2269–2275.
(7) Corderman, R. R.; Beauchamp, J. L. *Inorg. Chem.* **1977**, *16*, 3135–3139.
(8) Graham, W. A. G. *Inorg. Chem.* **1968**, *7*, 315–321.
(9) Angelici, R. J.; Ingemanson, C. M. *Inorg. Chem.* **1969**, *8*, 83–86.
(10) Darensbourg, D. J.; Brown, T. L. *Inorg. Chem.* **1968**, *7*, 959–966.
(11) Parshall, G. W. *J. Am. Chem. Soc.* **1966**, *88*, 704–708.

0002-7863/83/1505-7033$01.50/0